# Uniaxial Drawing of Isotactic Poly(acrylonitrile): Development of Oriented Structure and Tensile Properties

**Daisuke Sawai, Akira Yamane, Tunenori Kameda, and Tetsuo Kanamoto***

*Department of Applied Chemistry, Science University of Tokyo, Kagurazaka, Shinjuku-ku, Tokyo 162-8601, Japan*

**Masayoshi Ito**

*Department of Chemistry, Science University of Tokyo, Kagurazaka, Shinjuku-ku, Tokyo 162-8601, Japan*

**Hitoshi Yamazaki and Kunio Hisatani**

*Fundamental Research Laboratory of Fibers and Fiber-Forming Polymers, Asahi Chemical Industry Co. Ltd., 11-7 Hacchonawate, Takatuki, Osaka 569, Japan*

*Received March 4, 1999; Revised Manuscript Received June 22, 1999*

ABSTRACT: Uniaxial drawing of isotactic poly(acrylonitrile) (iso-PAN, isotactic triad fraction of 68%) and the resultant structure and tensile properties of drawn products were studied. The results were compared to those of atactic-PAN (at-PAN). Dried gel films prepared from 2 to 10 wt % solutions in *N*,*N*′-dimethylformamide were initially drawn by solid-state coextrusion (first-stage draw) to an extrusion draw ratio of 16, followed by a further tensile draw at 100−200 °C (second-stage draw). The ductility of iso-PAN increased rapidly above 100 °C, due to the onset of molecular motion in crystalline regions, as found by WAXD at elevated temperatures. In contrast, the ductility of at-PAN increased above the first-order crystal/crystal transition at around 150 °C. Thus, the temperature for optimum second-stage draw of iso-PAN, 130−140 °C, was significantly lower than that (160−180 °C) of at-PAN, reflecting their crystal softening temperatures. The maximum achieved total draw ratios ($DR_t$), after the two-stage draw, were comparable for these PANs. The shapes of stress/strain curves for highly drawn products recorded at room temperature were significantly different between iso- and at-PAN. The meridional WAXD patterns of these samples revealed that the difference is ascribed to their chain conformations which change with the applied tensile stress. The iso-PAN likely takes a predominantly 3/1 helical chain conformation, whereas at-PAN seems to consist of both planar zigzag and helical sequences, as previously suggested. However, upon increasing the tensile stress on oriented fibers, the helical sequences progressively transform into a planar zigzag conformation which shows a higher modulus. Such an effect of the stress was more prominent in at-PAN than in iso-PAN fibers. Thus, the maximum achieved tensile modulus, as well as the modulus at a given $DR_t$, was slightly higher for iso-PAN than for at-PAN (28.5 ± 1.0 vs 23.0 ± 1.0 GPa). However, the maximum tensile strength at the break was comparable for each PAN, at 0.90 ± 0.05 GPa.

## Introduction

During the past decade, extensive research has been made on the structure and properties of atactic poly(acrylonitrile) (at-PAN). PAN is an unusual polymer in that even an atactic sample can crystallize; thus, the chain conformation is expected to be imperfect for at-PAN. Indeed the crystal structure of at-PAN has been the subject of controversy. Some authors[1,2] propose a paracrystalline structure with hexagonal (or pseudohexagonal) chain packing and no order along the chain direction (a two-dimensional lattice), based on wide-angle X-ray diffraction (WAXD) patterns. Others[3,4] report an orthorhombic unit cell with three-dimensional order. Bashir, in a review,[5] concluded that the orthorhombic cell is due to the cocrystallization of PAN with polar solvents. He reports that it transforms into the hexagonal cell with no order along the chain direction upon drying or drawing.

Although a number of articles have been published on at-PAN fibers, only a few studies have been reported on the structure and properties of iso-PAN.[6−9] Kamide et al.[6] have shown that highly isotactic poly(acrylonitrile) (iso-PAN) can be prepared by $\gamma$-irradiation polymerization of AN within a urea canal complex. Yamazaki et al.[7] report that this polymer takes an orthorhombic chain packing with unit cell constants of $a = 1.07$ and $b = 1.21$ nm, based on the electron diffraction pattern of a solution-grown single crystal. Liu and Ruland[8] propose a 3/1 helical chain conformation for iso-PAN and predominantly planar zigzag conformation for at-PAN, based on their two-dimensional Fourier transform analysis of WAXD patterns of PAN fibers. Hu et al.[9] have also shown that the WAXD meridional peaks at around $2\theta = 40°$ and 36° (Cu K$\alpha$) of at-PAN fibers are ascribed to the helical conformation of isotactic sequences and to the planar zigzag conformation of syndiotactic sequences, respectively.

In previous papers,[10,11] we have shown that gel films of high-molecular-weight at-PAN exhibit high ductility in a two-stage draw, and even PAN has a fairly high chain stiffness and a high cohesive energy density due to the bulky nitrile groups with a large dipole.[12] The maximum achieved total draw ratio ($DR_t$) and tensile properties increased with sample molecular weight ($M_v$).[11] The highest $M_v$ at-PAN ($M_v = 2.3 \times 10^6$)

* To whom correspondence should be addressed.

10.1021/ma990334c CCC: $18.00 
Published on Web 08/04/1999

**Table 1. Characteristics of iso- and at-PAN Samples**

| sample | $M_v$ | triad tacticity | | | sol conc (%) | $DR_{t,max}$[a] | $T_{d,opt}$ (°C)[b] |
|---|---|---|---|---|---|---|---|
| | | *mm* | *mr* | *rr* | | | |
| iso-PAN | $5.2 \times 10^5$ | 0.68 | 0.22 | 0.10 | 2 | 66 | 130 |
| | | | | | 10 | 40 | 140 |
| at-PAN | $4.4 \times 10^5$ | 0.25 | 0.51 | 0.24 | 2 | 71 | 170 |
| | | | | | 10 | 44 | 180 |

[a] The maximum achieved draw ratio at the optimum drawing temperature. [b] The optimum drawing temperature for the second-stage draw.

exhibited maximum tensile modulus and strength of 28.5 and 1.6 GPa, respectively, at a $DR_t$ of 100−130. Such highly drawn samples show an extreme morphology, which is indicated by a high chain orientation function ($f_c = 0.996$) and a high tensile modulus, comparable to the yet uncertain X-ray crystal modulus (28 GPa).[13] Furthermore, it was found that ultraoriented samples exhibit a first-order crystal/crystal transition from orthorhombic to hexagonal chain packing around 150 °C, as determined by the temperature variations of the X-ray equatorial reflections,[11] differential scanning calorimetry (DSC), and dynamic mechanical analysis (DMA).[14]

In this work, dried gel films of iso- and at-PAN with comparable $M_v$'s of around $5 \times 10^5$ were drawn using a two-stage draw.[15] The effects of chain configuration on the drawing of gel films and the resultant structure and tensile properties of drawn products were studied. These results are discussed in relation to the crystal softening temperatures and the chain conformations which change with the chain configuration and application of stress on fibers of iso- and at-PAN.

## Experimental Section

**Polymerization.** The iso-PAN used was prepared by $\gamma$-irradiation polymerization of AN within a urea canal complex[6] at Asahi Chemicals Co., Ltd. The at-PAN was prepared by suspension polymerization, as reported in previous papers.[10,11]

The intrinsic viscosity was measured in dimethyl sulfoxide at 50 °C. The viscosity average molecular weights ($M_v$) of iso- and at-PAN were calculated to be $5.2 \times 10^5$ and $4.4 \times 10^5$, respectively, according to an intrinsic viscosity/molecular weight relation.[16]

Triad tacticity, (*mm*), (*mr*), and (*rr*), was determined from the intensities of three methine-carbon peaks of a $^{13}C$ NMR spectrum.[17] The *mm* calculated from NMR spectra were 25% for the at-PAN and 68% for the iso-PAN, as summarized in Table 1.

**Gel Films.** Polymer solutions with concentrations of 2, 5, and 10 wt % were prepared by dissolving the requisite amounts of PAN in *N*,*N*′-dimethylformamide at 100 °C. The hot solutions were then transferred into stainless trays and quenched at 0 °C for 2 h to make gels. The wet gel films were extracted with methanol and then dried at room temperature in vacuo to constant weights.

**Two-Stage Drawing.** The dry gel films of PAN prepared from the lowest solution concentration of 2 wt % were brittle and showed low ductility on straight tensile draw. However, the gel films were ductile on solid-state coextrusion.[18] Thus, the extruded films were further drawn by a tensile force at elevated temperatures to achieve a higher draw. For the first-stage solid-state coextrusion, a gel film 0.15 mm thick, 5 mm wide, and 60 mm long was placed between two split billet halves of high-density polyethylene, and the assembly was coextruded at 125 °C through a conical brass die with a nominal extrusion draw ratio (EDR) of 6−20. EDR was determined from the separation of ink marks preimprinted on the surface of the gel film. The extrudates, thus prepared, were further drawn (second-stage draw) by a tensile force at a draw temperature ($T_d$) of 100−200 °C in an air oven equipped with an Orientec Tensilon tensile tester HTM-100 at constant crosshead speeds (CHS). The draw ratio (DR) for the second-stage draw was also determined from the deformation of ink marks. The total draw ratio ($DR_t$) was defined by $DR_t$ = (first-stage EDR) × (second-stage DR).

**Characterization.** Wide-angle X-ray diffraction (WAXD) patterns were recorded photographically by a flat plate camera and by diffractometer scans. Photographs were obtained with Cu Kα radiation generated at 40 kV and 25 mA on a Rigaku Gigerflex RAD-3A, monochromatized by a graphite monochromator. Diffraction profiles were recorded by a transmission mode with Ni-filtered Cu Kα radiation generated at 40 kV and 150 mA on a Rigaku Rotaflex RU-200 rotating anode X-ray generator, equipped with a diffractometer and a pulse height discriminator. The azimuthal intensity distribution was recorded by step scans at 0.1° intervals in azimuthal angle, using a Rigaku fiber specimen holder with a first collimator of $\phi$ = 0.5 mm and a receiving slit of 1.8° ($2\theta$ direction) × 0.3° (azimuthal direction). The counting time was adjusted to accumulate to a peak intensity of $\sim 10^4$ counts. The crystalline chain orientation was evaluated by the Herman orientation function, $f_c$.[19]

The densities of drawn products were measured at 30 ± 0.1 °C in a density gradient column consisting of mixtures of *n*-heptane and carbon tetrachloride.

The tensile modulus and strength on the fiber axis were measured at strain rates of $1 \times 10^{-3}$ and $1 \times 10^{-2}$, respectively, at room temperature, with the measurements being made at least three times for a given sample. The modulus was determined from the initial slope of the stress/strain curve at a low strain (<0.1%). The cross-sectional area of a sample was calculated from the sample weight, length, and measured density.

## Results and Discussion

**Drawing.** In a previous work[10] on the ultradrawing of at-PAN gel using a two-stage draw technique, it was found that the drawability and uniformity of the resultant drawn products are sensitive to several factors, including the solution concentration from which the gel was made (chain entanglement density), first-stage EDR, and the second-stage draw temperatures. Therefore, in the drawing of iso-PAN, the effects of these drawing variables on the second-stage tensile draw were examined. When an extrudate of a low EDR ≤ 12 was tensile-drawn, the draw became unstable above a specific temperature, depending on the initial EDR. For an extrudate with a higher EDR of 16 or 20, uniform deformation proceeded in the whole range of $T_d$ studied (≤200 °C). Such an effect of the initial EDR on the drawing of iso-PAN gel films is similar to that previously found in at-PAN.[10] Thus, in this work, an EDR of 16 was chosen as the starting EDR for the second-stage tensile draw of both iso- and at-PAN.

Parts a and b of Figure 1 respectively show nominal stress/strain curves for the second-stage tensile draw of EDR 16 extrudates, prepared from 2 and 10 wt % gel films of iso-PAN, recorded at different $T_d$'s. The solution concentration of 2 wt % corresponds to the lowest one from which a coherent gel film was obtained for the iso-

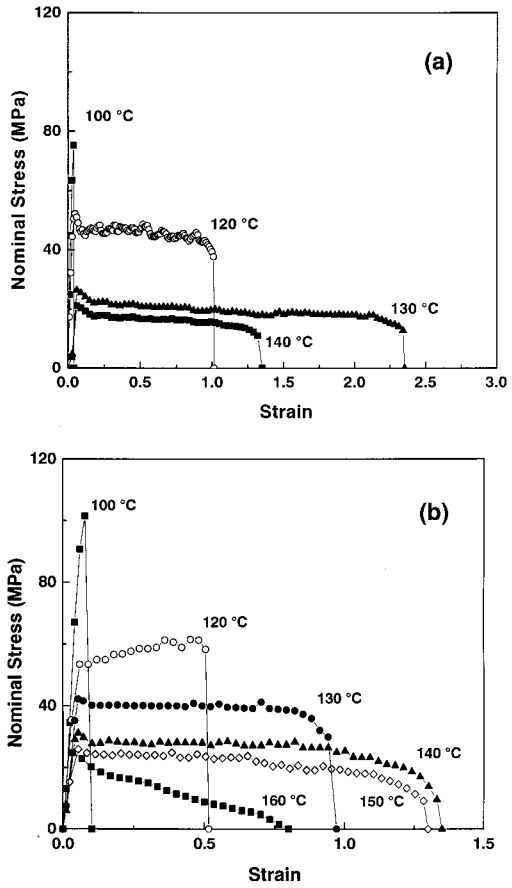


**Figure 1.** Nominal stress/strain curves for the second-stage drawing of iso-PAN recorded at different $T_d$'s: (a) 2 wt % gel and (b) 10 wt % gel. The draw temperatures are shown in the figure.

PAN sample. The draw stress significantly decreased, and the strain before failure markedly increased with increasing $T_d$ and/or decreasing the concentration of solution from which the gel had been prepared. At a specific $T_d$, the draw stress after yielding remained nearly constant until failure occurred. The increase in gel ductility with decreasing prior solution concentration suggests that the chain entanglement density, which may decrease when decreasing the prior solution concentration,[20] also controls the ductility of iso-PAN, which has a fairly high chain stiffness and a strong intermolecular interaction due to the bulky nitrile groups with a large dipole.[12]

Figure 2 shows the maximum achieved $DR_t$ ($DR_{t,max}$) as a function of $T_d$ for the second-stage tensile draw of iso-PAN gel films, prepared from 2 to 10 wt % solutions. Similar data for at-PAN were also included for comparison. The $DR_{t,max}$ for iso-PAN increased rapidly with $T_d$ above 100 °C, reaching a maximum at a specific $T_d$, which increased with the solution concentration from which the gel had been made. At yet a higher $T_d$, it decreased again. The effect of $T_d$ on ductility is more prominent for the gel prepared from the lowest solution concentration of 2 wt %, which likely has the lowest entanglement density. The $DR_{t,max}$ of iso- and at-PAN at their optimum $T_d$'s were comparable. However, the optimum $T_d$ for iso-PAN, 130−140 °C, is 30−40 °C lower than that of 160−180 °C for at-PAN, when compared for gels prepared from the same solution concentrations. It has been shown that the ductility of crystalline polymers increases above any crystalline relaxation or

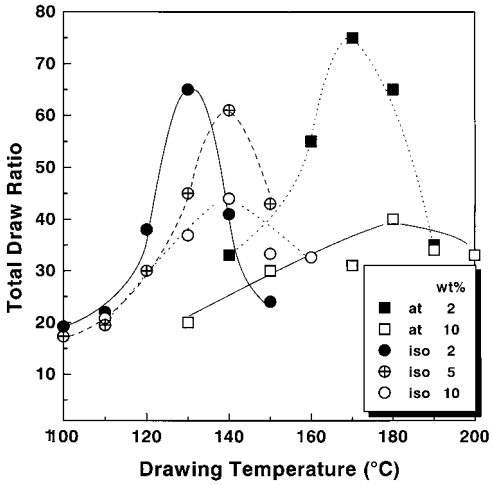


**Figure 2.** Maximum achieved $DR_t$ as a function of second-stage draw temperature $T_d$ for gels prepared from 2 to 10 wt % solutions of iso- and at-PAN. The symbols are explained in the figure.

crystal/crystal transition temperature.[21−23] Consistent with this, our previous study[10,11] on the drawing of at-PAN showed that $DR_{t,max}$ increased rapidly above the crystal/crystal first-order thermal transition at 150 °C, detected by WAXD and DSC.[10,14] Thus, the rapid increase in $DR_{t,max}$ above 100 °C for iso-PAN suggests the likely existence of a crystalline relaxation or crystal/crystal transition around 100 °C. Because no articles are available on the thermal transitions in iso-PAN crystals, WAXD measurements on iso-PAN fibers were carried out at elevated temperatures.

**Wide-Angle X-ray Diffraction at Elevated Temperatures.** DMA data of at-PAN fibers generally exhibit two major relaxations around 150 and 100 °C at 110 Hz, which are attributed to the molecular motion in amorphous regions and that in (para)crystalline regions, respectively.[24] In our previous DMA study on highly drawn at-PAN fibers,[14] it was found that the loss tangent peak at 150 °C consists of contributions from both the molecular motions in amorphous regions and the crystal/crystal transition detected by WAXD.[10] It was also found that highly drawn at-PAN fibers exhibit a DSC endothermic peak around 150 °C due to the crystal/crystal transition.[14] Thus, DSC scans were made on iso-PAN fibers with a $DR_t$ of 1−50. However, no such thermal transition was observed in iso-PAN fibers. The existence of the first-order thermal transition in at-PAN fibers and the absence of such a transition in iso-PAN fibers are likely related to their chain conformations,[8,9] as discussed later.

Figure 3 shows the temperature dependence of the lattice spacings of the equatorial reflection around $2\theta = 17°$ both for iso-PAN fibers with an EDR = 16 and a $DR_t = 50$ and for an at-PAN fiber with a $DR_t = 50$. The reflection of iso-PAN corresponds to the (120, 200) reflection of the orthorhombic unit cell.[7] The linear expansion coefficient of iso-PAN perpendicular to the chain axis, calculated from these data, increased from $\alpha = 9.23 \times 10^{-5}$/°C below 100 °C to $\alpha = 16.2 \times 10^{-5}$/°C above this temperature, suggesting an onset of molecular motion in crystalline regions. In sharp contrast to iso-PAN fibers, the (110) and (200) reflections of the orthorhombic cell[10] for the at-PAN fiber transformed into the $(100)_h$ reflection of the hexagonal cell at 150 °C, indicating the occurrence of a phase transition from

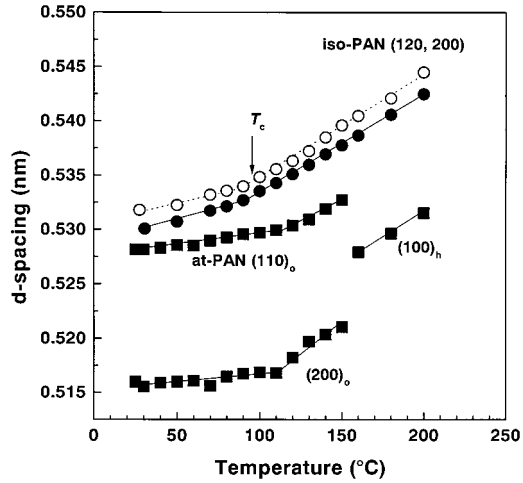


**Figure 3.** Temperature variations of the orthorhombic (120, 200) spacing for iso-PAN fibers with an EDR = 16 (○) and a $DR_t$ = 40 (●). Changes of the orthorhombic $(110)_o$ and $(200)_o$ spacings and the hexagonal $(100)_h$ spacing of a highly drawn at-PAN fiber with a $DR_t$ of 40 are also shown for comparison (■).

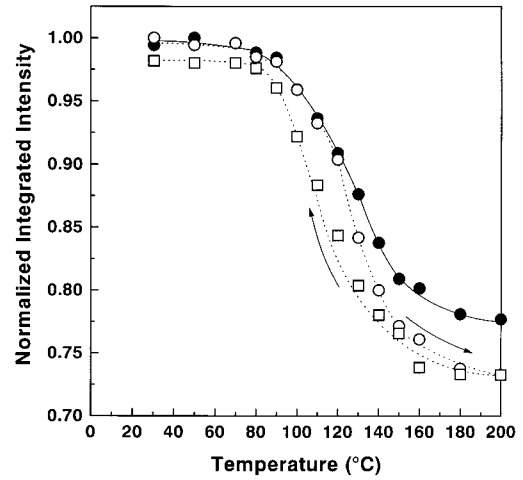


**Figure 4.** Temperature dependence of the normalized integrated intensity for the orthorhombic (120, 200) reflection of iso-PAN fibers with an EDR = 16 (●) and a $DR_t$ = 50 (○) recorded in the heating process. The intensity change of the (120, 200) reflection in cooling process is also shown for the fiber with a $DR_t$ = 50 (□).

orthorhombic to hexagonal chain packing.[10] Figure 4 shows the temperature dependence of the WAXD integrated intensity of the (120, 200) reflection for these iso-PAN samples. On heating, the intensity decreased rapidly from 90 to 180 °C, suggesting again an onset of molecular motion in crystalline regions above 90 °C and a rapid increase in chain mobility with further increasing temperature. On cooling, the intensity increased rapidly from 180 to 90 °C and then reverted back to a constant intensity close (~97%) to the initial intensity below 80 °C. This indicates that the thermal transition of iso-PAN at 100 °C found in this work is reversible with respect to the temperature. The existence of this thermal transition in crystalline regions well explains the rapid increase in ductility above this temperature due to the crystal softening (see Figure 2).

**Tensile Properties.** Figure 5 shows the room-temperature tensile modulus as a function of $DR_t$ for extrusion and two-stage drawing of iso- and at-PAN gels prepared from different solution concentrations. The

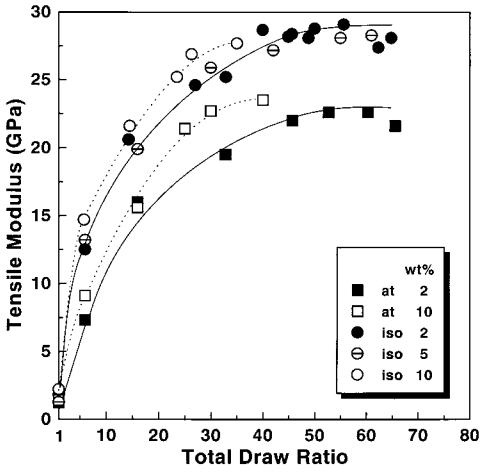


**Figure 5.** Tensile modulus as a function of $DR_t$ for two-stage drawing of iso- and at-PAN gels prepared from different solution concentrations of 2 (●), 5 (⊖), and 10 wt % (○) for iso-PAN and 2 (■) and 10 wt % (□) for at-PAN.

second-stage tensile draw was carried out at the optimum draw temperature, giving the highest $DR_t$, for each gel film. The modulus of 2 wt % gel films increased rapidly with $DR_t$ and approached constant value characteristics for iso- and at-PAN at $DR_t \geq 50$. There was a slightly more rapid modulus increase for the drawing of gel films prepared from a higher solution concentration of 10 wt % than those prepared from a lower solution concentration. Although the former gels exhibited lower drawability, the maximum achieved modulus was comparable to those achieved for the highly drawable latter gels. This suggests that a gel prepared from a higher solution concentration may have a higher entanglement density, which leads to lower ductility but higher efficiency of draw as evaluated by the modulus vs $DR_t$.

The modulus at a given $DR_t$ is somewhat higher for iso-PAN than for at-PAN. Because the $DR_{t,max}$ is comparable for these two PANs, the maximum achieved tensile modulus is also slightly higher for iso-PAN than for at-PAN, 28.5 vs 23 GPa. Such a difference in the moduli is likely related to the chain conformation of these PANs, as will be discussed later based on the meridional WAXD.

The theoretical crystal modulus of iso-PAN has not been reported. Sakurada et al.[25] calculated the force required to stretch a polymer chain by 1% ($f$ value) for various polymers, based on the elastic moduli of crystals in the chain direction and the cross-sectional area of a chain. They showed that the $f$ values for various polymers are predominantly determined by the conformation of crystalline chains with a minor contribution from intermolecular interactions. Indeed, the $f$ values for isopolypropylene (iso-PP) and isopolybutene-1 (iso-PB-1), both having a 3/1 helical conformation, are 1.18 and 1.11 dyn, respectively.[25] By applying this rule to iso-PAN which has 3/1 helical conformation,[8,9] the crystal modulus in the chain direction was estimated. The cross-sectional area of an iso-PAN chain is 0.324 nm$^2$, as calculated from the unit cell dimensions of $a$ = 1.06, $b$ = 1.22 nm with four chains penetrating a cell, as discussed later. The crystal modulus calculated by assuming an $f$ value of 1.15 dyn, as an average of the $f$ values for the two polymers, is 35 GPa for fully iso-PAN. The maximum modulus of 28.5 GPa achieved by ultradrawing of the iso-PAN sample is slightly lower than

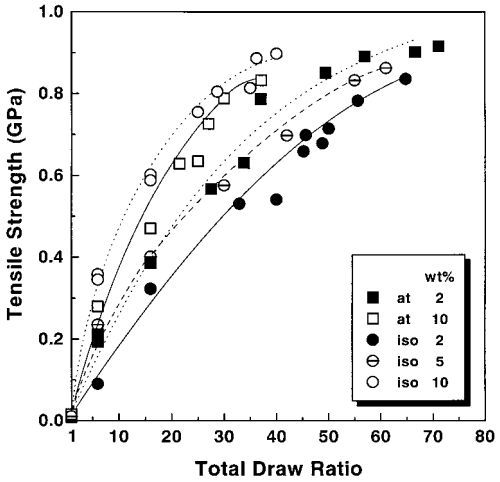


**Figure 6.** Tensile strength as a function of $DR_t$ for two-stage drawing of iso- and at-PAN gels prepared from different solution concentrations. The symbols are the same as in Figure 5.

that estimated for a perfectly isotactic PAN, probably due to the existence of configurational defects in the iso-PAN sample used in this work ($^{13}C$ NMR triad isotacticity of 68%, see Table 1).

Figure 6 shows tensile strength vs $DR_t$ for a two-stage draw of iso- and at-PAN gel films. The strength for both polymers increased rapidly with $DR_t$ in the lower range, reaching a maximum of 0.85−0.92 GPa at the highest achieved $DR_t$ of 40−70, depending on the solution concentrations. In both iso- and at-PAN, the strength upon draw increased most rapidly with $DR_t$ for the gel prepared from the highest solution concentration of 10 wt %, as also observed in modulus vs $DR_t$ (Figure 5). However, the maximum achieved strength was comparable to that achieved for the highly drawable gel prepared from the lowest solution concentration of 2 wt %.

**Structure and Morphology Development.** Although the general features of WAXD patterns of iso-PAN fibers are similar to those of at-PAN fibers,[8−11] a closer examination revealed some differences between them in the equatorial reflection around $2\theta = 17°$ and meridional scattering around $2\theta = 40°$.

Figure 7 shows WAXD patterns of iso-PAN for a draw ratio series prepared from a 2 wt % gel film. The patterns taken with the incident X-ray beam, which was both parallel and perpendicular to the film surface, were identical. The initial gel film of iso-PAN shows Debye−Scherrer rings around $2\theta = 17°$ and 30°, overlapped with a fairly strong diffuse scattering from disordered regions. With increasing $DR_t$, the reflections became gradually sharper, and the azimuthal intensity distribution concentrated on the equator. High chain orientation and high crystallinity are indicated by the sharp reflection spots on the equator for a highly drawn fiber of a $DR_t = 65$ (Figure 7d).

The high-resolution diffractometer scans for iso-PAN fibers (not shown) showed that the equatorial reflection around $2\theta = 17°$ consists of a single sharp peak, which is indexed as the (120, 200) reflection assuming the orthorhombic cell proposed by Yamazaki et al.[7] In contrast, the equatorial reflection around $2\theta = 17°$ for a highly drawn at-PAN fiber consists of two peaks at $2\theta = 16.8°$ and 17.2°, corresponding respectively to the

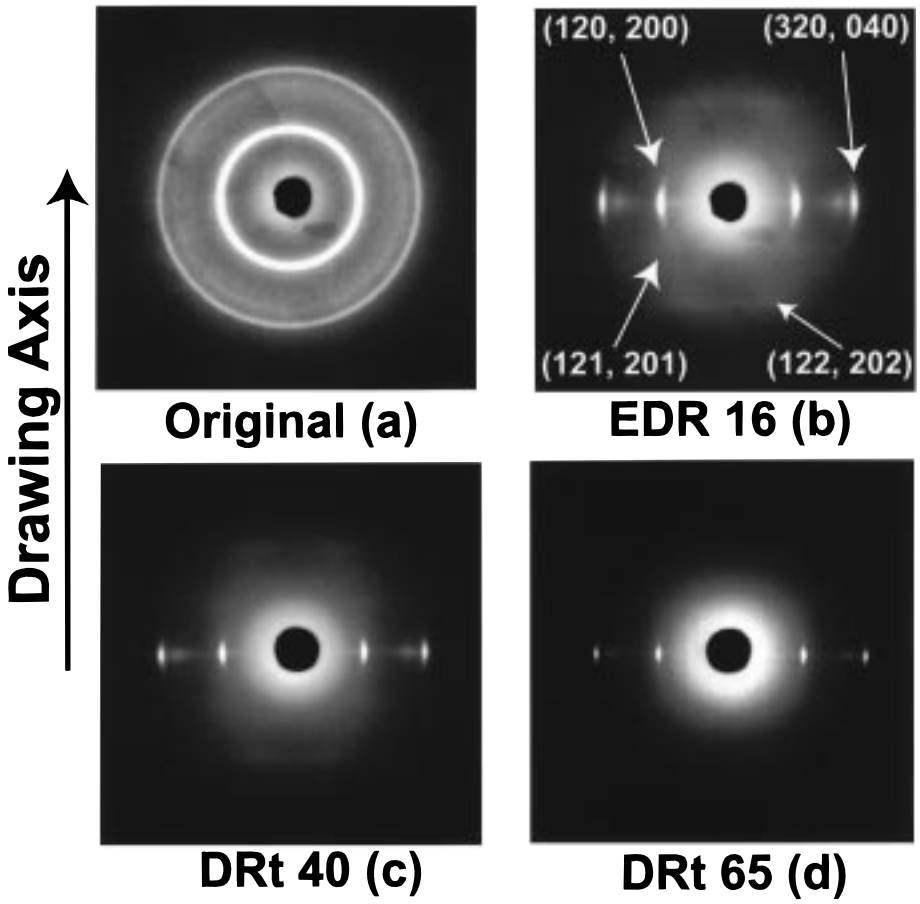


**Figure 7.** WAXD patterns of a draw ratio series for an iso-PAN gel: (a) original 2 wt % gel, (b) EDR = 16, (c) $DR_t = 40$, and (d) $DR_t = 65$.

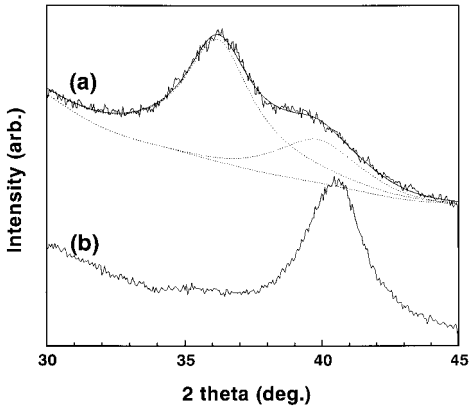


**Figure 8.** WAXD meridional scans around $2\theta = 40°$ for (a) at-PAN and (b) iso-PAN fibers with a $DR_t = 40$.

(200) and (110) reflections of the orthorhombic chain packing.[10] These facts indicate that the chain packing mode is somewhat different between iso- and at-PAN. The equatorial reflection at $2\theta = 30°$ for iso-PAN in Figure 7 is ascribed to the (040, 320) reflection. The unit cell parameters calculated from these reflections are $a = 1.06$ and $b = 1.22$ nm, in good agreement with those determined from the electron diffraction of a single crystal.[7] It is noted that the off-equatorial reflections in Figure 7, which could be indexed as the (121, 201) and (122, 202) reflections, were also observed in all the drawn samples, although these reflections were significantly broader than those of the equatorial ones. This suggests the existence of significant disorder along the chain axis for iso-PAN, as observed for at-PAN fibers.[8,9,11]

Figure 8 compares the high-resolution diffractometer scans on the meridian around $2\theta = 40°$ for highly drawn iso- and at-PAN fibers with a $DR_t = 40$. The scattering pattern of the at-PAN fiber shows two peaks at $2\theta = 36.3°$ and 39.7°, which correspond to the spacings of 0.247 and 0.227 nm, respectively.[10,11] These peaks were ascribed to the scatterings from the zigzag (syndiotactic and short isotactic) and the helical (long isotactic) sequences, respectively.[9] In contrast, the meridional scan for the iso-PAN fiber shows a single sharp peak at $2\theta = 40.4°$, corresponding to a spacing of 0.223 nm. This peak could be indexed as the (003) reflection of a unit cell with a 3/1 helical conformation of iso-PAN chains[8] or scattering from helical sequences of isotactic segments.[9] Further, it is noted that the fiber period of 0.67 nm calculated from the spacing of this meridional scattering is in good agreement with that of iso-PP (0.65 nm), having a 3/1 helix conformation.[26]

Comparing the fiber densities and those calculated from unit cell constants shows that four chains penetrate a unit cell. Thus, the crystal structure of the iso-PAN used here (isotactic triad fraction of 68%) is approximated by an orthorhombic unit cell with $a = 1.06$, $b = 1.22$, and $c = 0.67$ nm, in which four chains are included and significant disorder exists along the chain axis. Alternatively, the structure can be expressed by a two-dimensional orthorhombic lattice with unit cell constants of $a = 1.06$ nm and $b = 1.22$ nm and an average monomer repeat distance of $c = 0.223$ nm.

The crystalline chain orientation was evaluated by the Herman orientation function,[19] $f_c$, calculated from the azimuthal intensity distribution of the (120, 200) reflection, assuming a fiber symmetry. Further, it was also

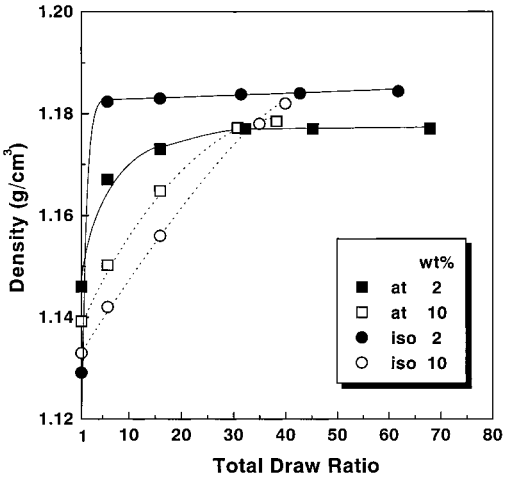


**Figure 9.** Density as a function of $DR_t$ for two-stage drawing of iso- and at-PAN gels prepared from 2 to 10 wt % solutions. The symbols are the same as in Figure 5.

assumed that the azimuthal intensity distributions are predominantly determined by the orientation distribution of the chain axis, with minor contribution from the crystallite size and disorder along the fiber axis, which might broaden the equatorial reflection perpendicular to the equator. The $f_c$ increased rapidly with $DR_t$ in the lower region and reached a maximum value of $f_c = 0.992-0.996$ at higher $DR_t$'s $\geq 30$, depending on the prior solution concentrations from which gels were made for both iso- and at-PANs.

Figure 9 shows density as a function of $DR_t$ for a two-stage draw. Although the crystallinity could not be calculated from the sample density, as neither the amorphous nor the crystal densities are known for either iso- or at-PAN, the observed density change with $DR_t$ can be a measure of the structural change upon drawing. The density of an iso-PAN gel prepared from a 2 wt % solution increased suddenly on solid-state coextrusion to a low EDR of 6 from the initial $\rho = 1.13$ g/cm$^3$ to a limiting value of 1.184 g/cm$^3$. Further drawing of the gel led to no increase in the density. In contrast, the density of a gel film prepared from a higher solution concentration of 10 wt % increased more slowly but steadily with $DR_t$, reaching a maximum of 1.179 g/cm$^3$ at the highest $DR_t$ of 40. At-PAN gel films also showed similar increases in density with $DR_t$, depending on the solution concentrations from which the gels had been made.

The observed maximum fiber density of 1.184 g/cm$^3$ for iso-PAN is slightly higher than that of the 1.179 g/cm$^3$ for at-PAN fibers. As discussed in a previous paper,[11] these values are significantly larger than the crystal density of 1.12 g/cm$^3$ calculated assuming a monomer repeat distance of 0.25 nm for a planar zigzag chain conformation. The theoretical crystal densities are 1.12 and 1.22 g/cm$^3$, estimated from the orthorhombic chain packing with unit cell constants of $a = 1.02$ and $b = 0.61$ nm with monomer repeat distances of 0.25 and 0.23 nm based on the meridional WAXD pattern of at-PAN fibers. Thus, the average crystal density of at-PAN should be between these two values, and indeed it is consistent with the observed fiber densities of 1.113–1.179 g/cm$^3$.

The theoretical crystal density of iso-PAN is 1.22 g/cm$^3$, calculated on the basis of an orthorhombic unit cell with cell constants of $a = 1.06$ and $b = 1.22$ nm

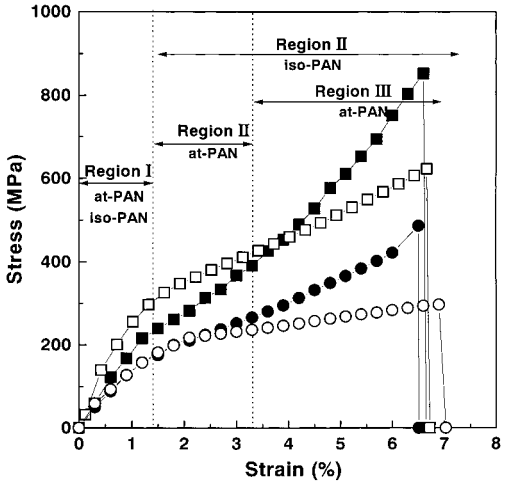


**Figure 10.** Stress/strain curves for iso- and at-PAN fibers recorded at room temperature. Iso-PAN fibers with an EDR = 16 (○), $DR_t = 40$ (□) and at-PAN fibers with an EDR = 16 (●), $DR_t = 40$ (■).

with a monomer repeat distance of 0.223 nm (or $c$ = 0.67 nm for the 3/1 helix). The appearance of a weak scattering around $2\theta = 36°$ in addition to the main peak at $2\theta = 40.3°$ (Figure 8) suggests that the average crystal density may be only slightly lower than 1.22 g/cm$^3$, but still close to this value. This estimate is also consistent with the observed fiber densities of 1.123−1.184 g/cm$^3$ for iso-PAN, which are somewhat higher than those of at-PAN fibers.

**Effect of Chain Configuration on the Stress/Strain Behavior.** It was shown that iso-PAN and syndiotactic PAN take helical and planar zigzag chain conformations, respectively,[8,9] based on computer simulations of the two-dimensional WAXD patterns. Hu et al.[9] also suggested that at-PAN fibers consist of both the helical (isotaicic) and planar zigzag (syndiotactic and short atactic) sequences. Further, Liu and Ruland[8] proposed the occurrence of kinks in at-PAN, which interrupt the planar zigzag sequences. Thus, they explained the lower crystal modulus of at-PAN, which is 1 order of magnitude lower than what would be expected for planar zigzag conformation, based on the existence of such kinks.

The tensile modulus at a given $DR_t$ determined at low strain (<0.1%), as well as the maximum achieved modulus, was somewhat higher for iso-PAN than for at-PAN (Figure 5). This is likely related to the chain conformations of the two PAN,[8,9] which may affect the stress/strain behavior of oriented samples, and hence the crystal modulus. Figure 10 shows stress/strain curves recorded at room temperature for iso- and at-PAN fibers with an EDR of 16 and a $DR_t$ of 40. The curves of highly drawn fibers exhibit characteristic features depending on their chain configurations. The stress/strain curve of the highly drawn iso-PAN fiber is characterized by two distinct regions. In the lower strain region (strain <1.5%, region I), the stress increases rapidly with strain. In the higher strain region (strain >1.5%, region II), the stress increases more slowly and linearly with strain. In contrast, the curve of a highly drawn at-PAN fiber is characterized by three distinct regions. Region I is in the strain range <1.5% where the stress increases rapidly with strain, while region II is in the strain range from 1.5 to 3.5% where the stress increases more slowly and linearly. At yet a higher strain >3.5% (region III), the stress again increases more rapidly with strain. Thus, at-PAN fibers are characterized by the appearance of region III, which is absent in iso-PAN fibers. Furthermore, the extensional stress for an iso-PAN fiber with a $DR_t$ of 40 was higher than that of an at-PAN fiber with the same $DR_t$ below a strain of 3.5%, but it became lower than that of the at-PAN fiber at yet a higher strain. Such stress/strain behavior characteristic for iso- and at-PAN is also observable for the extrudates with a lower EDR of 16, as shown in Figure 10. In view of the fact that the extent of plastic deformation was negligible for the tensile tests at room temperature, the characteristics of the stress/strain behavior for the highly oriented iso- and at-PAN fibers are likely related to the chain conformations of the two kinds of PAN.

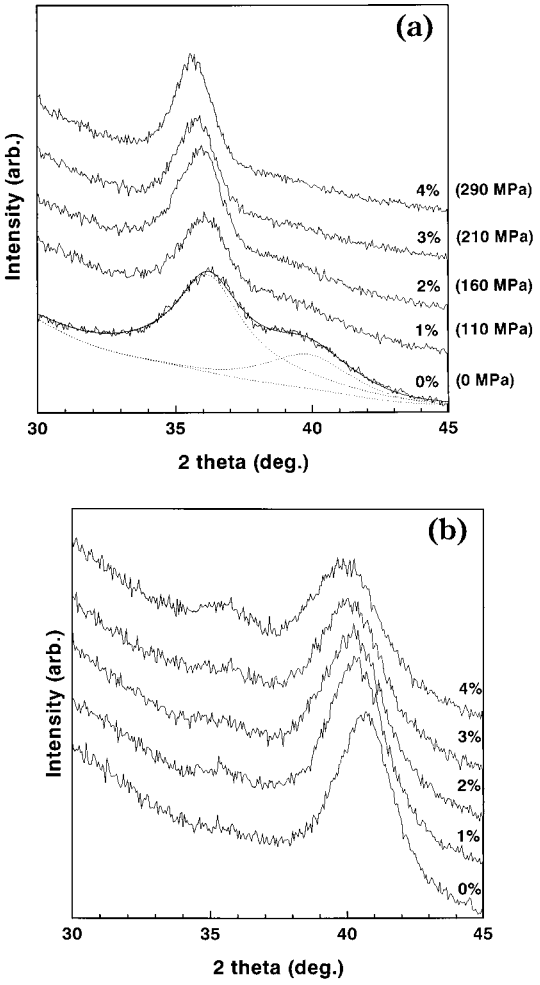


**Figure 11.** WAXD meridional scans at constant strains of 0−4% for (a) at-PAN and (b) iso-PAN fibers with a $DR_t = 40$. The stresses corresponding to the strains are also shown.

Parts a and b of Figure 11 show a series of the WAXD meridional profiles for at- and iso-PAN fibers, respectively, with a $DR_t$ of 40, recorded at a constant strain of 0−4% and room temperature. When a fiber was elongated to a certain strain, the stress gradually decreased due to relaxation and approached a constant value characteristic of the applied strain and the sample $DR_t$ after 30 min. Thus, WAXD measurements were made 30 min after the application of a strain.

As shown in Figure 11a, the WAXD meridional scan of the at-PAN fiber with no strain shows a fairly strong peak at $2\theta = 36.3°$ (peak I) and a weak one at 39.7°

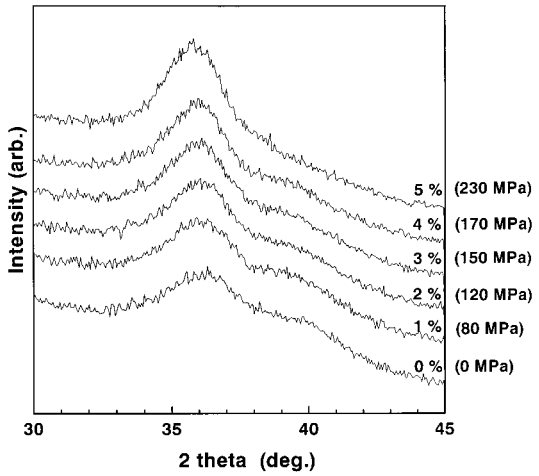


**Figure 12.** WAXD meridional scans for at-PAN with an EDR = 16 at constant strains of 0−5%. The stresses corresponding to the strains are also shown.

(peak II). It should be remembered that the former corresponds to the scattering from planar zigzag sequences and the latter from helical ones.[8,9] Upon successive strain increases, peak I shifted to a lower angle, and its intensity increased at the expense of the intensity of peak II. Peak II completely disappeared at strain ≥3%, suggesting that the at-PAN fiber predominantly takes a planar zigzag conformation above this strain level. In contrast, the meridional pattern of the iso-PAN fiber with no strain (Figure 11b) shows only peak II at $2\theta = 40°$, indicating that the chains predominantly take a helical conformation. Upon straining, peak II shifted to a lower angle, and peak I around $2\theta = 36°$ appeared and grew slowly at the expense of the intensity of peak I. However, the intensity of peak I of the iso-PAN fiber was remarkably weaker than that of the at-PAN fiber even at the highest strain of 4%, indicating the iso-PAN fiber takes a predominantly helical conformation even at a 4% strain. These observations indicate that some sequences initially having helical conformation transform into planar zigzag conformation upon the application of strain.

Such conformational changes with strain well explain the characteristic shapes of the stress/strain curves of iso- and at-PAN fibers in Figure 10. The stress/strain behavior in region I is commonly observed for oriented fibers of crystalline polymers. The slower increase of the stress in region II is likely ascribed in part to the conformational transformation of some helical sequences to planar zigzag ones under increasing strain. Region III in Figure 10 was observed after most of the initially helical sequences had transformed into planar zigzag conformations in the highly drawn at-PAN fiber at a strain of 3 % (see Figure 11a). As the planar zigzag conformation may give a higher modulus than the helical conformation, the more rapid increase of the stress in region III is consistent with the conformational change with strain for the highly drawn at-PAN fiber.

In increasing the applied strain, the stress measured after relaxation to a constant value increased, as shown in Figure 11a. To determine whether the strain or the stress is the crucial factor promoting the conformational change, the effect of strain and the corresponding stress on the WAXD meridional profile are compared for at-PAN fibers showing different moduli (and hence draw ratio). Figure 12 shows the effects of strain and the corresponding stress for an extrudate with a lower EDR of 16. The intensity of peak II at $2\theta = 40°$ from the helical sequences decreased with increasing strain and completely disappeared on straining by 5%, which corresponds to a stress of 230 MPa. For the fiber with a higher $DR_t$ of 40 (Figure 11a), peak II disappeared at a lower strain of 3%, which exhibited a stress of 210 MPa, comparable to the stress at which the peak II disappeared in the EDR 16 extrudate (Figure 12). This fact implies that the transformation from helix to planar zigzag conformation is primarily induced by the extensional stress applied on these samples. This is further supported by the fact that the two samples with different DRs show similar WAXD profiles at a comparable stress level.

## Conclusions

Dried gel films prepared from 2 to 10 wt % solutions of iso- and at-PAN having a comparable $M_v$ of $\sim 5.0 \times 10^5$ were uniaxially drawn by a two-stage draw under a wide range of draw conditions. The optimum draw condition for a gel film of PAN was found to depend markedly on the chain configuration, as well as on the solution concentration from which the gel had been made. However, the $DR_{t,max}$ under the optimum draw condition was comparable in each PAN. The ductility of iso-PAN increased rapidly above $T_d > 100$ °C due to the onset of molecular motion in crystalline regions at 100 °C, determined by WAXD measurements at elevated temperatures. In contrast, the ductility of at-PAN increased above 150 °C, due to the existence of a crystal/crystal first-order transition. The stress/strain behavior at room temperature for highly drawn fibers was markedly affected by the chain conformation which changes with the chain configuration and stress imposed on the fibers. At- and iso-PAN fibers under no stress seem to take predominantly planar zigzag and helical conformations, respectively, as predicted by computer simulations.[8,9] Helical sequences in a highly drawn at-PAN fiber transformed into planer zigzag conformation upon the application of stress. Such an effect of stress on the chain conformation was not significant in iso-PAN fibers. The maximum achieved tensile modulus, as well as the modulus at a given $DR_t$, is slightly higher for iso-PAN than for at-PAN (28.5 vs 23.0 GPa). However, the maximum achieved tensile strength was not affected by the chain configuration and was 0.9 GPa for both iso- and at-PAN. The crystal structure of the iso-PAN used here can be approximated by an orthorhombic two-dimensional lattice with unit cell constants of $a = 1.06$ nm and $b = 1.22$ nm and an average monomer repeat distance of 0.223 nm, having four chains penetrating a cell and significant disorder along the chain axis. The chain seems to take a predominantly 3/1 helical conformation, as suggested.[8,9]

**Acknowledgment.** This work was partly supported by the Grant-in-Aid from Ministry of Education, Science and Culture of Japan (#11650934). D.S. expresses his appreciation for the JSPS Research Fellowship for Young Scientists.

## References and Notes

(1) Bohn, C. R.; Schaefgen, J. R.; Statton, W. O. *J. Polym. Sci.* **1961,** *55*, 31.
(2) Holland, V. F.; Mitchell, S. B.; Hunter, W. L.; Lindenmeyer, P. H. *J. Polym. Sci.* **1962**, *62*, 145.
(3) Hinrichsen, G.; Orth, H. *Kolloid-Z. Polym.* **1971**, *247*, 844.

(4) Kumamaru, F.; Kajiyama, T.; Takayanagi, M. *J. Cryst. Growth* **1980,** *48*, 202.
(5) Bashir, Z. *J. Polym. Sci., Polym. Phys. Ed.* **1994,** *32*, 1125.
(6) Kamide, K.; Yamazaki, H.; Miyazaki, Y. *Polym. J.* **1986**, *18*, 819.
(7) Yamazaki, H.; Kajita, S.; Kamide, K. *Polym. J.* **1987**, *19*, 995.
(8) Liu, X. D.; Ruland, W. *Macromolecules* **1993**, *26*, 3030.
(9) Hu, X.; Johnson, D. J.; Tomka, J. G. *J. Text. Inst.* **1995**, *86*, 322.
(10) Yamane, A.; Sawai, D.; Kameda, T.; Kanamoto, T.; Ito, M.; Porter, R. S. *Macromolecules* **1997**, *30*, 4170.
(11) Sawai, D.; Yamane, A.; Takahashi, H.; Kanamoto, T.; Ito, M.; Porter, R. S. *J. Polym. Sci., Polym. Phys.* **1998**, *36*, 629.
(12) Krigbaum, W. R.; Tokita, N. *J. Polym. Sci.* **1960**, *43*, 647.
(13) Allen, R. A.; Ward, I. M.; Bashir, Z. *Polymer* **1994**, *35*, 4035.
(14) Sawai, D.; Kanamoto, T.; Porter, R. S. *Macromolecules* **1998**, *31*, 2010.
(15) Kanamoto, T.; Tsuruta, A.; Tanaka, K.; Takeda, M.; Porter, R. S. *Macromolecules* **1988**, *21*, 470.
(16) Kamide, K.; Yamazaki, H.; Miyazaki, Y. *Polym. J.* **1987**, *19*, 995.
(17) Kamide, K.; Yamazaki, H.; Okajima, K.; Hikichi, K. *Polym. J.* **1985**, *17*, 1233.
(18) Griswald, P. D.; Zachariades, A. E.; Porter, R. S. *Polym. Eng. Sci.* **1978**, *18*, 861.
(19) Alexander, L. E. *X-ray Diffraction Methods in Polymer Science*; John Wiley & Sons: New York, 1969.
(20) Smith, P.; Lemstra, P. J.; Booij, H. C. *J. Polym. Sci., Phys. Ed.* **1981**, *19*, 877.
(21) Takayanagi, M. *Koubunshi (High Polym. Jpn.)* **1966**, *10*, 289.
(22) Aharoni, S. M.; Sibilia, J. P. *J. Appl. Polym. Sci.* **1979**, *23*, 133.
(23) Saraf, R.; Porter, R. S. *J. Polym. Sci., Polym. Phys. Ed.* **1988**, *26*, 1049.
(24) Minami, S. *J. Polym. Sci., Appl. Polym. Symp.* **1974**, *25*, 145.
(25) Sakurada, I.; Kaji, K. *J. Polym. Sci., Part C* **1970**, *31*, 57.
(26) Natta, G.; Corradini, P.; Bassi, I. W. *Nuovo Cim. Suppl.* **1960**, *15*, 52.

MA990334C